Atmospheric
Measurement
Techniques

Measurement of ambient NO_3 reactivity: design, characterization and first deployment of a new instrument

Jonathan M. Liebmann, Gerhard Schuster, Jan B. Schuladen, Nicolas Sobanski, Jos Lelieveld, and John N. Crowley

Atmospheric Chemistry Department, Max-Planck-Institut für Chemie, 55128 Mainz, Germany

Correspondence to: John N. Crowley (john.crowley@mpic.de)

Abstract. We describe the first instrument for measurement of the rate constant (s^{-1}) for reactive loss (i.e., the total reactivity) of NO_3 in ambient air. Cavity-ring-down spectroscopy is used to monitor the mixing ratio of synthetically generated NO_3 ($\approx$ 30–50 pptv) after passing through a flow-tube reactor with variable residence time (generally 10.5 s). The change in concentration of NO_3 upon modulation of the bath gas between zero air and ambient air is used to derive its loss rate constant, which is then corrected for formation and decomposition of N_2O_5 via numerical simulation. The instrument is calibrated and characterized using known amounts of NO and NO_2 and tested in the laboratory with an isoprene standard. The lowest reactivity that can be detected (defined by the stability of the NO_3 source, instrumental parameters and NO_2 mixing ratios) is $0.005 \, s^{-1}$. An automated dilution procedure enables measurement of NO_3 reactivities up to $45 \, s^{-1}$, this upper limit being defined mainly by the dilution accuracy. The typical total uncertainty associated with the reactivity measurement at the center of its dynamic range is 16 %, though this is dependent on ambient NO_2 levels. Results from the first successful deployment of the instrument at a forested mountain site with urban influence are shown and future developments outlined.

1 Introduction

Large amounts of biogenic and anthropogenic trace gases are emitted annually into the atmosphere. Recent estimates (Guenther et al., 2012) suggest that about 1000 Tg of biogenic volatile organic compounds (VOCs), especially isoprene (contributing 50 %) and monoterpenes (15 %), are emitted annually by vegetation. The global burden of anthropogenic emission is dominated by CO_2, CO, N_2O, CH_4, SO_2, NO_2 and organic carbon, the latter contributing about 11 Tg (Huang et al., 2015). In particular, nitrogen oxides from combustion and microbial activity in soils have a major impact on the chemistry of the natural atmosphere (Crutzen, 1973). Most VOCs are oxidized efficiently in the Earth's boundary layer, the oxidizing capacity of which represents 15 % of that of the entire atmosphere (Lelieveld et al., 2016). Biogenic and anthropogenic VOCs have a significant impact on air quality and human health and knowing and understanding their lifetimes, which are determined by the oxidizing capacity of the atmosphere, is a prerequisite to predicting future atmospheric composition and related climate phenomena (Lelieveld et al., 2008).

During daytime, photochemically formed OH radicals represent the dominant contribution to the oxidative capacity of the atmosphere. As OH levels are vastly reduced in the absence of sunlight, the NO_3 radical (formed by reaction of NO_2 with O_3; Reaction R1) is the major oxidizing agent at elevated NO_x for many biogenic terpenoids and other unsaturated compounds at nighttime (Wayne et al., 1991; Atkinson, 2000; Atkinson and Arey, 2003a, b; Brown and Stutz, 2012; Ng et al., 2017).
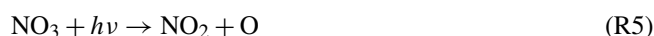
$$NO_2 + O_3 \rightarrow NO_3 + O_2 \tag{R1}$$

NO_3 reacts rapidly with NO (Reaction R2, rate constant $2.6 \times 10^{-11} \, cm^3 \, molecule^{-1} \, s^{-2}$ at 298 K; Atkinson et al., 2004) and undergoes rapid photolysis (Reactions R5, R6) so that its lifetime is usually of the order of seconds during the day and its concentration too low for it to be considered an important daytime oxidant.

At night, NO_3 can react with NO_2, forming N_2O_5, which thermally decomposes to set up a thermal equilibrium between NO_2, NO_3 and N_2O_5 (Reactions R3, R4) with N_2O_5

formation favored by lower temperatures. As both NO$_3$ and N$_2$O$_5$ are formed from NO$_x$ (NO$_x$ = NO + NO$_2$) the loss of either NO$_3$ via gas-phase reactions or N$_2$O$_5$ via heterogeneous uptake to particles or deposition implies a reduction in NO$_x$, and thus a reduction in the rate of photochemical O$_3$ formation (Dentener and Crutzen, 1993). In addition, heterogeneous loss of N$_2$O$_5$ can also result in release of ClNO$_2$ from chloride-containing particles (Reaction R7) (Osthoff et al., 2008; Thornton et al., 2010; Mielke et al., 2011; Phillips et al., 2012; Riedel et al., 2012). The main loss processes of NO$_3$ are summarized in Fig. 1.

$$NO_3 + NO \rightarrow 2NO_2 \tag{R2}$$

$$NO_2 + NO_3 + M \rightarrow N_2O_5 + M \tag{R3}$$

$$N_2O_5 + M \rightarrow NO_3 + NO_2 + M \tag{R4}$$

$$NO_3 + h\nu \rightarrow NO_2 + O \tag{R5}$$

$$NO_3 + h\nu \rightarrow NO + O_2 \tag{R6}$$

$$N_2O_5 + \text{surface} \rightarrow NO_3^- \quad \text{(and/or ClNO}_2\text{)} \tag{R7}$$

In rural and forested areas, reaction with biogenic VOCs can dominate the loss of NO$_3$ (Mogensen et al., 2015). Especially terpenoids like limonene ($k = 1.2 \times 10^{-11}$ cm^3 molecule^{-1} s^{-1}), α-pinene ($k = 6.2 \times 10^{-12}$ cm^3 molecule^{-1} s^{-1}) and isoprene ($k = 6.5 \times 10^{-13}$ cm^3 molecule^{-1} s^{-1}) have high rate constants for reaction with NO$_3$ (IUPAC, 2016; Ng et al., 2017). In such environments, when NO$_x$ levels are low, NO$_3$ mixing ratios may be sub-pptv and below the detection limit for most instruments (Rinne et al., 2012).

The reaction of NO$_3$ with trace gases containing unsaturated C=C bonds proceeds via addition to form nitrooxyalkyl radicals that undergo rapid reaction with O$_2$ to form nitrooxyalkyl peroxy radicals. The peroxy radicals react further (with HO$_2$, NO, NO$_2$ or NO$_3$,) to form multifunctional organic nitrates, which can contribute to generation and growth of secondary organic aerosols (Fry et al., 2014; Ng et al., 2017) or be lost by deposition.

The role of NO$_3$ as an oxidizing agent may be assessed via its total reactivity (or inverse lifetime). Whereas for OH, experimental methods for measuring total reactivity in ambient air exist (Kovacs and Brune, 2001; Sinha et al., 2008), NO$_3$ reactivity has not yet been directly measured. Stationary-state approximations have often been used to calculate NO$_3$ lifetimes from its mixing ratio and production rate, the latter being given by k_1[NO$_2$][O$_3$] (Heintz et al., 1996; Geyer and Platt, 2002; Brown et al., 2007a, b, 2009; Sobanski et al., 2016b). Thus the stationary-state turnover lifetime, τ_{ss}, can be calculated according to Eq. (1), where k_1 is the rate constant for Reaction (R1).

$$k_{ss} = \frac{1}{\tau_{ss}} = \frac{k_1 [O_3][NO_2]}{[NO_3]} \tag{1}$$

This method is applicable when the chemical lifetime of NO$_3$ is sufficiently short so that stationary state can be achieved
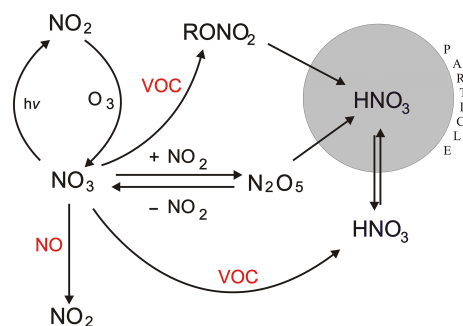

Figure 1. Gas-phase formation and loss of tropospheric NO$_3$, indicating processes which transfer reactive nitrogen to the particle phase. RONO$_2$ are alkyl nitrates. VOC is volatile organic compound.

within transport time from emission to measurement location (Brown et al., 2003). Formally it is achieved when the production and loss of NO$_3$ and N$_2$O$_5$ are balanced (Brown et al., 2003; Crowley et al., 2011). The time to acquire stationary state depends on production and loss rates for NO$_3$ and N$_2$O$_5$ and can take several hours. This approach can break down under conditions of moderate to high NO$_2$ levels, strong sinks, low temperatures or very clean air masses in which the sinks for NO$_3$ and N$_2$O$_5$ become small (Brown et al., 2003). Indeed, Sobanski et al. (2016b) observed much lower stationary-state loss rates compared to those calculated from measured VOC mixing ratios during the PARADE 2011 campaign and concluded that this was mainly the result of sampling from a low-lying residual layer with VOC emissions that were too close for NO$_3$ concentrations to achieve stationary state. They also considered the possibility that NO$_3$ may be formed by the oxidation of NO$_2$ by Criegee intermediates, which would bias calculations of its reactivity.

Summarizing, NO$_3$ reactivity with respect to gas-phase losses is an indication of nighttime oxidation rates of VOCs, with direct impacts on NO$_x$ levels by forming long-lived reservoir species (alkyl nitrates), some of which will partition to the particle phase. Via modification of N$_2$O$_5$ concentrations (formed in an association reaction of NO$_3$ with NO$_2$, Reaction R3), the NO$_3$ reactivity indirectly controls heterogeneous NO$_x$ losses and ClNO$_2$ formation rates.

In this paper we describe a newly developed instrument that enables point measurements of NO$_3$ reactivity in ambient air. After introducing the methodology in Sect. 2, we show the results of extensive laboratory characterization of the instrument along with discussion of the uncertainties associated with those measurements in Sects. 3 to 5. In Sect. 6 we present a data set of ambient NO$_3$ reactivity obtained at a forested/urban location in southwestern Germany.
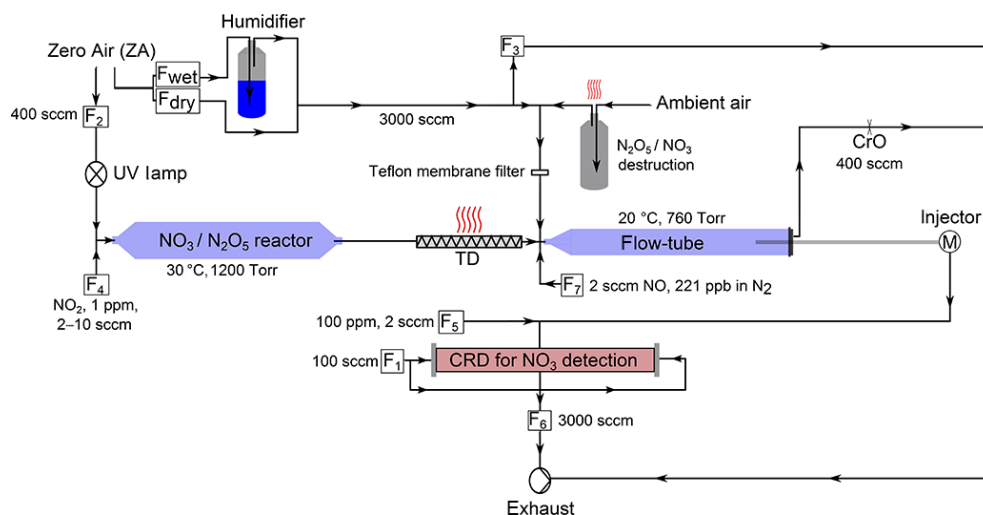
Figure 2. Schematic diagram of the NO$_3$-reactivity measurement. F$_1$–F$_7$ are mass flow controllers: F$_1$ is mirror purge flow, F$_2$ is zero air for O$_3$ generation, F$_3$ is dilution/inlet overflow (switching between zero air and ambient), F$_4$ is NO$_2$ for NO$_3$/N$_2$O$_5$ generation, F$_5$ is NO titration of NO$_3$, F$_6$ is cavity flow to pump and F$_7$ is NO flow for online reactivity calibration. CrO is critical orifice. TD is heated tubing for thermal decomposition of N$_2$O$_5$ to NO$_3$ at 140 °C.

2   Methodology

Our experiments to measure NO$_3$ reactivity involve comparison of loss rates of synthetically generated NO$_3$ in zero air and in ambient air introduced into a flow-tube reactor. In zero air, the loss of NO$_3$ is due to its reaction with NO$_2$ (present as a necessary component in the generation of NO$_3$, see below) and losses on surfaces of the flow tube. When zero air is replaced by ambient air, NO$_3$ is additionally removed by reaction with reactive gases present and its mixing ratio reduced accordingly. An analysis of the change in signal for a fixed reaction time enables the NO$_3$ reactivity to be derived once certain corrections have been applied (see below).

Figure 2 displays a schematic diagram of the experimental setup. The three central components are a dark reactor for generation of NO$_3$, the flow tube in which NO$_3$ reacts with trace gases in ambient air samples and the detection system for NO$_3$.

2.1   Generation of NO$_3$

Many laboratory studies of NO$_3$ kinetics have used the thermal decomposition of N$_2$O$_5$ as NO$_3$ source (Reaction R4) (Wayne et al., 1991). The generation of NO$_3$ from gas-phase N$_2$O$_5$ eluted from samples of crystalline N$_2$O$_5$ (at −80 °C) was found to be insufficiently stable for the present application and is also difficult (though not impossible; see, e.g., Fuchs et al., 2008; Wagner et al., 2011) to use during field campaigns where adequate laboratory facilities for the safe generation and purification of N$_2$O$_5$ are frequently not available. In addition, generation of NO$_3$ from N$_2$O$_5$ was also accompanied by an NO$_2$ impurity of several parts per billion (ppbv).

We therefore generate NO$_3$ and N$_2$O$_5$ in situ, via the oxidation of NO$_2$ by O$_3$ (Reactions R1, R3). For this purpose, 400 standard cm^3 min^{-1} (sccm) of synthetic air from a zero-air generator (Fuhr Cap 180) is passed over a Hg lamp (low-pressure, Penray type) at a pressure of 1200 Torr. The photo-dissociation of O$_2$ at 184.95 nm results in formation of oxygen atoms that recombine with O$_2$ to form ≈ 400 ppbv O$_3$. The O$_3$/air flow is then mixed with NO$_2$ in synthetic air (0.93 ppmv, 1–10 sccm) and directed into a temperature-stabilized (30 °C), darkened, FEP-coated reactor (length 70 cm, diameter 6 cm) also at a pressure of 1200 Torr. The reactor is darkened to prevent the photolysis of NO$_3$ by room lights. Operation at above-ambient pressure extends the reaction time for a given flow rate, thus optimizing the conversion of NO$_2$ to NO$_3$ via the reaction between NO$_2$ and O$_3$, which has a low rate constant of 4.05 × 10^{-17} cm^3 molecule^{-1} s^{-1} at 30 °C. The use of high pressures also optimizes the formation of N$_2$O$_5$ in the termolecular Reaction R3 and reduces the rate of diffusion and loss of NO$_3$ to the walls of the reactor. A high pressure in the darkened reactor also has the advantage of partially decoupling it from fluctuations in ambient pressure which influence the formation of N$_2$O$_5$. Heating the reactor to above room temperature is carried out to stabilize the formation of N$_2$O$_5$, which otherwise shows strong fluctuations owing to variations in laboratory temperature, typically about 3–5° within the course of a day or night. The approximate reaction time for the stepwise conversion of NO$_2$ to N$_2$O$_5$ in the darkened reactor is ≈ 5 min. Based on the O$_3$ concentration and the rate constant for Reaction (R1), the initial conversion of NO$_2$ to NO$_3$ is about 15 %.

The gas exiting the darkened reactor passes through a pinhole ($\emptyset \approx 250\,\mu m$) to reduce the pressure to roughly ambient level and then enters a ≈ 30 cm long piece of 1/4 in. (≈ 6.4 mm) PFA tubing (residence time ≈ 0.5 s), which is heated to $140\,°C$ in order to thermally decompose N_2O_5 to NO_3. Calculations using the thermal decomposition rate constant for N_2O_5 (lifetime of 0.001 s at $140\,°C$) indicate that after ≈ 0.1 s the N_2O_5 is stoichiometrically converted to NO_3. The temperature is measured on the outside of the PFA tubing and does not necessarily reflect the temperature of the gas flowing through it. The value of $140\,°C$ is chosen based on a series of experiments in which the tubing temperature was varied and the yield of NO_3 monitored. A PFA T-piece located immediately behind the heated tubing is used to add a 2900 sccm flow of either zero or ambient air to the synthetic NO_3 sample. After this dilution step the air contains ≈ 30–50 pptv NO_3, ≈ 1 ppbv NO_2 and ≈ 50 ppbv O_3. As described later, keeping NO_2 and O_3 levels as low as possible has important consequences for the data analysis. Low levels of NO_3 also help to ensure that the addition of NO_3 does not significantly change the reactivity of the air, i.e., by removing a large fraction of the reactive trace gases (RTG). We later assess the potential change in air-mass reactivity (i.e., by depletion of RTG or formation of reactive radicals) following addition of NO_3 at these levels to ambient air.

As described below, the present instrument is a modification of one designed to measure ambient mixing ratios of NO_3 and N_2O_5 and is equipped with a second cavity connected to a heated inlet that measures the sum of NO_3 and N_2O_5. Experiments in which both cavities were used to analyze the flow out of the heated piping indicated that there was no residual N_2O_5.

2.2 Detection of NO_3 using cavity-ring-down spectroscopy (CRDS)

For detection of the NO_3 radical we used CRDS, a sensitive technique for measurements of atmospheric trace gases and often used for measurement of ambient NO_3 (Brown et al., 2002). In essence, CRDS is an extinction measurement in a closed optical resonator (cavity) where light is trapped between mirrors with high reflectivity to generate a very long absorption path. Ring-down refers to the decay of light intensity (monitored behind the cavity exit mirror) and the general expression to derive the concentration of an absorbing or scattering gas is given by (Berden et al., 2000)

$$[X] = \frac{1}{c\sigma_{(x,\lambda)}}\left(\frac{1}{\tau_X} - \frac{1}{\tau_0}\right), \tag{2}$$

where τ_0 and τ_x correspond to inverse-decay constants in the absence and presence of an absorbing or scattering trace gas X, respectively, and $\sigma_{(X,\lambda)}$ is the absorption cross section/scattering coefficient of X at wavelength λ.

The instrument used is a two-channel CRDS that was previously used to measure ambient levels of N_2O_5 and NO_3

(Schuster et al., 2009; Crowley et al., 2010). Important modifications to the previous setup include use of FEP-coated glass cavities of equivalent size and fibre optics for the coupling of the laser to the cavity. The thermal dissociation cavity previously used for detection of atmospheric N_2O_5 is not necessary for the measurement of NO_3 lifetimes but was used for calibration and characterization experiments. Only the central features and important modifications compared to the prototype described in Schuster et al. (2009) are described in detail here.

The light source is a 625 Hz, square-wave modulated, 100 mW laser diode located in a Thorlabs TCLDM9 housing and thermally stabilized at $36\,°C$ using a Thorlabs ITC502 laser diode combi controller to produce light at 661.95 nm (0.5 nm full width at half maximum) and therefore close to the NO_3 absorption maximum. The effective cross section of NO_3 was calculated as 2.09×10^{-17} cm^2 molecule^{-1} by convoluting the temperature-dependent NO_3 absorption spectrum (Orphal et al., 2003; Osthoff et al., 2007) with the laser diode emission spectrum. Coupling between the laser diode and the cavities is achieved by using either optical fibres (0.22 NA, 50 μm core, 400–2400 nm) for measuring NO_3 reactivity or using fibre optics with a beam splitter (Thorlabs FCMM50-50A-FC, 50 : 50 ratio) in order to operate both cavities. The beam was collimated (Thorlabs FiberPort Collimator PAF-X-18-PC-A) and directed through an optical isolator (Thorlabs IO-3D-660-VLP), focused by a lens (Thorlabs A230TM-A) into the optical fibre and then collimated again to a beam diameter of about 6 mm before entering the cavity.

The NO_3 cavity (Teflon-coated glass (DuPont, FEP, TE 9568), length 70 cm, volume 79 cm^3) was operated at room temperature, while the N_2O_5 cavity was operated at $80\,°C$ with a pre-cavity section heated to $85\,°C$ in order to convert N_2O_5 to NO_3. The NO_3 cavity was connected to the flow tube using 1/8″ (≈ 3.2 mm) PFA tubing that lined the 1/4″ (≈ 6.4 mm) injector. The use of small-diameter tubing results in short transport times between the flow tube and CRDS and also induces a pressure drop of 133 mbar, so that the pressure in the cavity was 880 mbar. Gases entered the middle of the cavity via a T-piece and were pumped from the ends via a flow controller into the exhaust. The flow rates in both cavities were 3000 cm^3 (STP) min^{-1} (sccm), resulting in a residence time of approximately 1.6 s as calculated from the volume flow rate. Gas entering the CRDS detector always passed through a 2 μm membrane filter (Pall Teflo) to remove particles. Light exiting the cavities through the rear mirror was detected by a photomultiplier (Hamamatsu E717-500) which was screened by a 662 nm interference filter. The pre-amplified PMT signal was digitized and averaged with a 10 MHz, 12 bit USB scope (Picoscope 3424) which was triggered at the laser modulation frequency of 625 Hz.

The ring-down constant in the absence of NO_3 was obtained by adding NO (1–3 sccm of a 100 ppmv mixture NO in N_2) every 40 points of measurement for approximately

15 s. Titration with NO took place at the inlet of the T-shaped glass cavity, giving the gas mixture sufficient time to react with NO$_3$. The L/d ratio (the ratio of the distance between the cavity mirrors, L, and the length of the cavity that is filled by absorber, d) was determined as described previously (Schuster et al., 2009; Crowley et al., 2010) and was 1.01 ± 0.03. Values of τ_0 in dry zero air at 760 Torr were usually between 140 and 160 µs, indicating optical path lengths of ≈ 42–48 km. When operated at a flow of 3000 sccm, the noise levels on the NO$_3$ signal are such that the precision (3 s integration interval) is better than 1 pptv. As we describe later, the NO$_3$ reactivity is derived from measurements of the relative change in the NO$_3$ mixing ratio, so that the precision rather than total uncertainty in the NO$_3$ mixing ratio defines the accuracy of the reactivity measurement.

2.3 Flow tube for NO$_3$ reactivity measurement

The flow tube, thermostated to 20 °C by flowing water through an outer jacket, is an FEP-coated glass tube of length 50 cm and internal diameter 4 cm. Gas enters the flow tube at one end via a conical section with a 3/8 in. (≈ 9.5 mm) glass fitting through which 1/4 in. (≈ 6.4 mm) PFA tubing could be inserted. The total flow through the flow tube was 3300 sccm, consisting of 400 sccm from the darkened reactor and 2900 sccm zero air/ambient air. The flow and pressures indicated above result in a Reynolds number of ≈ 123 (i.e., laminar flow) in the cylindrical part of the flow tube, but with an entrance length (Le) to acquire laminar flow of 27 cm, indicating that the flow tube operates in a mixed turbulent/laminar flow regime.

$$\text{Le} = 0.112 r Re \tag{3}$$

Gases exit the flow tube via a length of 1/8 in. PFA tubing supported in an axially centered stainless steel tube (length 50 cm, diameter 1/4 in.) which could be translated along the major flow-tube axis, thus changing the contact (reaction) time between NO$_3$ and any reactive species or the flow-tube wall. In principal, this enables the dynamic range of the measurement to be adjusted (i.e., long contact times for low reactivity, short contact times for high reactivity) though we found that reactivity-dependent dilution of the ambient air was a better method to extend the dynamic range to high reactivities as very short reaction times were not possible due to a finite residence time in the CRDS detection system and to mixing effects in the flow tube. In order to prevent formation of a "dead volume" at the back of the flow tube beyond the tip of the outlet, 400 sccm was removed via a critical orifice to the exhaust pump. During measurement of NO$_3$ reactivity the extraction point was usually set for a reaction time of about 10.5 s, which was determined as described below.

As described later, to derive the NO$_3$ reactivity we compare its concentration in zero air to that in ambient air samples. We found that when switching between sampling ambient air and dry zero air, the resulting change in relative humidity caused an abrupt change in NO$_3$, which then slowly recovered towards its original value. Measurement of the wall loss rate of NO$_3$ in dry and humidified zero air by moving the injector (see below) revealed no substantial difference and we conclude that the change in NO$_3$ is due to wall loss at the point of mixing of NO$_3$ flows and the zero-air flow, which is very turbulent. In order to eliminate data loss while waiting for signals to stabilize following zeroing, we humidify the zero air to the same absolute humidity (± 2 %) as ambient. To do this, the ambient relative humidity was monitored by passing 100 sccm air over a sensor that recorded both temperature and relative humidity. The zero air was humidified by directing a variable fraction of the (constant) total flow through a 2 L gas wash bottle filled with HPLC-grade water. The relative humidity of the resulting mixture was matched to ambient levels by dynamic adjustment of the fractional flow passing through the wash bottle. The zero air used for purging the mirrors as well that used for NO$_3$ generation was not humidified.

In order to ensure that air from the zero-air generator was free of reactive gases that survived the catalytic purification process, we compared it to hydrocarbon-free, bottled synthetic air (Westfalen). No change in the concentration of [NO$_3$] could be observed when switching between zero air and bottled air, indicating that the zero-air generator was suitable. However, poisoning of the catalyst of the zero-air generator by amines, sulfides or thiols or contamination of the filters could potentially become problematic when using compressed, highly polluted ambient air.

Derivation of the effective reaction time and wall loss rate constant for NO$_3$

In flow tubes where radial, diffusive mixing of gases is rapid (i.e., at low pressures of He and "plug-flow" conditions), the effective reaction time can be close to that calculated from the volumetric flow rate once axial diffusion is accounted for (Howard, 1979). At higher pressures and laminar flow, reactions times are defined by the parabolic velocity distribution and extent of radial mixing whereas high-pressure flow tubes operated under turbulent conditions (Reynold numbers > 3000) plug flow can be achieved (Seeley et al., 1993; Donahue et al., 1996). According to the calculations of Reynolds numbers outlined above, our flow tube is not operated in either a pure laminar or turbulent regime, which can make accurate calculation of the reaction time difficult. Using the volumetric flow rate and flow-tube diameter, we calculate an average, linear velocity of the gas of 4.78 cm s^{-1} at 760 Torr and 298 K in the cylindrical section of the flow tube. This enables us to calculate the injector-position-dependent reaction time in the flow tube, which for 45 cm is 9.5 s. This should be regarded as an initial estimate of the true reaction time as it does not consider the non-cylindrical section of the flow tube (2.5 % of total volume), the radial distribution of velocities in the flow tube or mixing effects. A further additional

1.6 s must be added to this to take the average reaction time in the cavity into account (calculated from the cavity volume and the flow rate), resulting in an approximate, total reaction time of 11.1 s.

A further method to derive an "effective" or averaged reaction time is to add a short pulse of gas to the flow tube and monitor its arrival time at the detector. However, as NO$_3$ cannot be easily stored, we instead add a pulse of a reactant that removes NO$_3$. A syringe was therefore used to add a short pulse (0.1 cm^3 in < 0.5 s) of NO diluted in N$_2$ (0.22 ppbv) to the flow tube at the T-piece where the NO$_3$ source and zero air are mixed.

The resultant depletion in the NO$_3$ signal (measured at a time resolution of 0.35 s) displayed an inverted Gaussian form with an elongated flank after the minimum (Fig. 3) which can be attributed to non-isothermal effects, secondary flows and recirculation processes in the flow tube (Huang et al., 2017), which require fluid dynamics simulations to be fully characterized. The average reaction time, t, can however be derived from

$$t = \frac{\sum I_j t_j}{\sum I_j}, \tag{4}$$

where I_j is the signal recorded at each time step t_j.

In total, 25 experiments were conducted, resulting in an effective reaction time of 11.4 ± 0.5 s determined via Eq. (4). The two methods outlined above thus provide approximate values for the reaction time which are in good agreement (< 3 % deviation).

As the reaction time is a central parameter for calculating the NO$_3$ reactivity, a third method was employed, in which a known amount of NO was added at the usual mixing point and the depletion in NO$_3$ observed. As the rate constant for reaction of NO with NO$_3$ is known with an uncertainty (at room temperature) of 13 %, this should enable derivation of an effective reaction time that also takes all mixing effects (both in the flow tube and cavity) into account. In a series of experiments, known amounts NO were added to the 2900 sccm flow of zero air (via a calibrated mass flow controller) at the usual mixing point. In the absence of other processes which remove or form NO$_3$, its change in concentration upon adding NO is described by

$$[NO_3]_t = [NO_3]_0 \exp^{-(k_2[NO]+k_w+k_3[NO_2])t}, \tag{5}$$

where $[NO_3]_0$ and $[NO_3]_t$ are the concentrations of NO$_3$ before and after addition of NO, respectively. k_2 and k_3 are the rate constants for reaction of NO$_3$ with NO and NO$_2$, respectively, at the flow-tube/cavity temperature, k_w is the rate constant (s^{-1}) for loss of NO$_3$ at the flow-tube walls and t is the desired parameter. Rearranging, we get the simple Eq. (6), which shows that a plot of ln([NO$_3$]$_t$) versus [NO] should yield a slope of $k_2 t$, from which t can be derived using an evaluated and recommended value of k_2 (Atkinson et
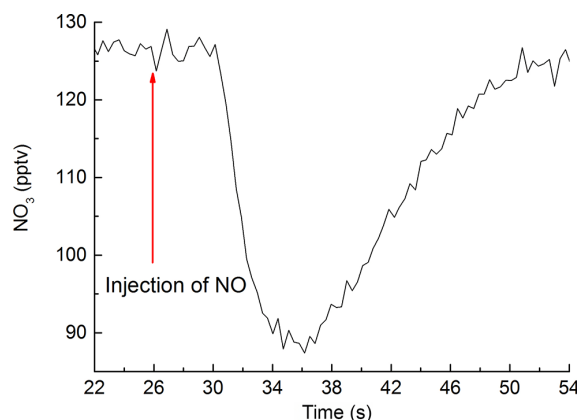

Figure 3. Derivation of effective reaction time by addition of a pulse (at $t = 26$ s) of NO using a syringe. The subsequent depletion in the NO$_3$ signal was analyzed using Eq. (4).

al., 2004). Once corrected for the contribution from $k_5[NO_2]$, the intercept should, in principal, give a value of k_w.

$$\ln\frac{[NO_3]_0}{[NO_3]_t} = (k_2[NO] + k_w + k_3[NO_2]) t \tag{6}$$

A plot of [NO$_3$]$_t$ versus [NO] is displayed in Fig. 4a for three different amounts of added NO$_2$. Although the curves follow roughly exponential behavior as expected, the slopes and thus the value of t obtained were found to depend on the initial NO$_2$ concentration, with values of 5.7, 5.1 and 4.5 s obtained for NO$_2$ mixing ratios of 2.94, 5.88 and 8.82 ppbv, respectively. This indicates that the kinetics of NO$_3$ formation and loss are more complex than defined by Eq. (6) and the relative rates of reaction of NO$_3$ with NO (Reaction R2) and NO$_2$ (Reaction R3) and its formation via N$_2$O$_5$ decomposition (Reaction R4) and reaction of O$_3$ with NO$_2$ (Reaction R1) in the flow tube all impact the NO$_3$ mixing ratio. In Fig. 4b we display the results of a similar experiment in which NO$_2$ as added. In this case, there is obvious curvature in the plot of [NO$_3$]$_t$ versus [NO$_2$], which is not predicted by Eq. (5). The decomposition of N$_2$O$_5$ formed by Reaction (R3) as well as oxidation of NO$_2$ by O$_3$ (Reaction R1, see Sect. 3) both lead to the formation of NO$_3$ and are the causes of this behavior, especially at high [NO$_2$] and low [NO]. At the flow-tube and cavity temperature (circa 298 K), the rate constant for decomposition of N$_2$O$_5$ (k_4) is 4.4×10^{-2} s^{-1} (Atkinson et al., 2004).

Extraction of the reaction time thus required numerical simulation of the data obtained by adding various amounts of NO to the flow tube in the presence of different NO$_3$ and NO$_2$ concentrations. The impact of Reactions (R2), (R3) and (R4) was assessed by numerical simulations using FACSIMILE (Curtis and Sweetenham, 1987) and considering the reactions listed in Table 1. The input parameters for the simulations were the concentrations of NO, NO$_2$ and O$_3$ and the rate constants, which were taken from IUPAC recommenda-

Table 1. FACSIMILE* simulations.

NO$_2$ + O$_3$ → NO$_3$ + O$_2$	$k_1 = 3.52 \times 10^{-17}$ cm^3 molecule^{-1} s^{-1}	k_1
NO$_3$ + NO → 2NO$_2$	$k_2 = 2.60 \times 10^{-11}$ cm^3 molecule^{-1} s^{-1}	k_2
NO$_3$ + NO$_2$ + M → N$_2$O$_5$ + M	$k_3 = 1.24 \times 10^{-12}$ cm^3 molecule^{-1} s^{-1}	k_3
N$_2$O$_5$ + M → NO$_2$ + NO$_3$ + M	$k_4 = 4.44 \times 10^{-2}$ cm^3 molecule^{-1} s^{-1}	k_4
NO + O$_3$ → NO$_2$ + O$_2$	$k_5 = 1.89 \times 10^{-14}$ cm^3 molecule^{-1} s^{-1}	k_5
NO$_3$ + wall → NO$_2$	$k_w = 4 \times 10^{-3}$ s^{-1}	k_w
k_{RTG}	variable/fitted	k_{RTG}

* For all simulations FACSIMILE/CHEKMAT (release H010 date 28 April 1987 version 1) was used. The rate constants (k_i) listed were taken from the IUPAC recommendations (Atkinson et al., 2004; IUPAC, 2016) at 298 K and 1 bar.
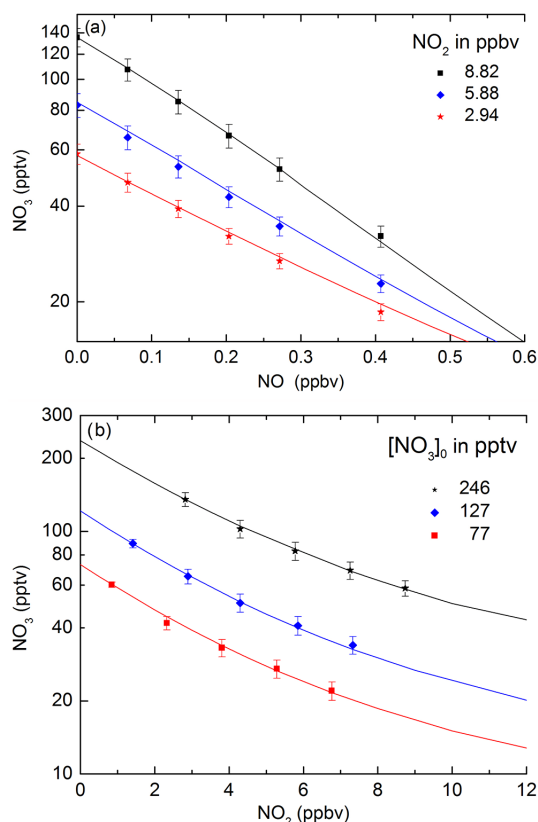

Figure 4. Characterization of the flow tube by numerical simulation of the NO$_3$ change following addition of NO and NO$_2$ at different mixing ratios. The symbols are measured NO$_3$ mixing ratios; the lines are the results of numerical simulations.

tions (Atkinson et al., 2004). The total reaction time (t) and the wall loss rate constant for NO$_3$ (k_w) were adjusted until each of the six data sets could be reproduced with a single value for each parameter. The initial concentration of [NO$_3$]$_0$ was allowed to float until best agreement was achieved. This way, the reaction time was determined to be 10.5 s, which is in good agreement with that derived by pulsed addition of NO. As our reactivity derivation relies on the change in NO$_3$ signal upon adding a reactant to the flow tube, we consider the value of 10.5 s, which takes mixing, diffusion, etc. into account, to be the most appropriate value but assign an uncertainty (± 1 s) that overlaps with the other methods. The wall loss rate of NO$_3$ (which is independent of the NO and NO$_2$ concentrations) was found to be 4×10^{-3} s^{-1}.

For analysis of ambient reactivity we use a reaction time of 10.5 s as derived from the addition of NO. This means that our ambient reactivities are directly tied to the rate constant for reaction between NO$_3$ and NO. As described later, during ambient measurements we periodically add a known amount of NO to the zero air to monitor a known reactivity under real operating conditions.

Figure 5a and b show the correlation between simulated and measured NO$_3$ concentrations in these experiments. In both cases the slope is close to unity (0.97–1.02) with an intercept close to zero. A set of similar experiments performed at 30 and 80 % humidity also showed excellent agreement using the same values of t and k_w. We conclude that the behavior of NO$_3$ in this system can be very accurately predicted by numerical simulations using a simple reaction scheme under a variety of conditions (initial NO$_3$, NO and NO$_2$ varied), giving us confidence in our ability to extract loss rates for NO$_3$ in ambient air.

When gas-phase reactivity is low, a substantial fraction of NO$_3$ may be lost via collisions with the walls rather than due to reactive gases. For this reason, we remeasured the value of k_w obtained above in a further set of experiments in which the NO$_3$ concentration was measured as a function of injector position (contact time in the flow tube) at a constant initial mixing ratio of NO$_3$ and NO$_2$ and in the absence of NO. For this we calculate the reaction time for each of the three injector positions from pulsed addition of NO as described above, but normalized to the reaction time derived from addition of NO with numerical simulation. The results of such an experiment are displayed in Fig. 6 and we draw attention to the fact that, even at maximum reaction time (10.5 s), the change in the NO$_3$ concentration is only about 10 %. This reflects the low efficiency of reaction of NO$_3$ with the FEP-coated glass walls. Similar experiments performed before and after the NOTOMO campaign (NOcturnal chemistry at the Taunus Observatorium: insights into Mechanisms of Oxidation) (see
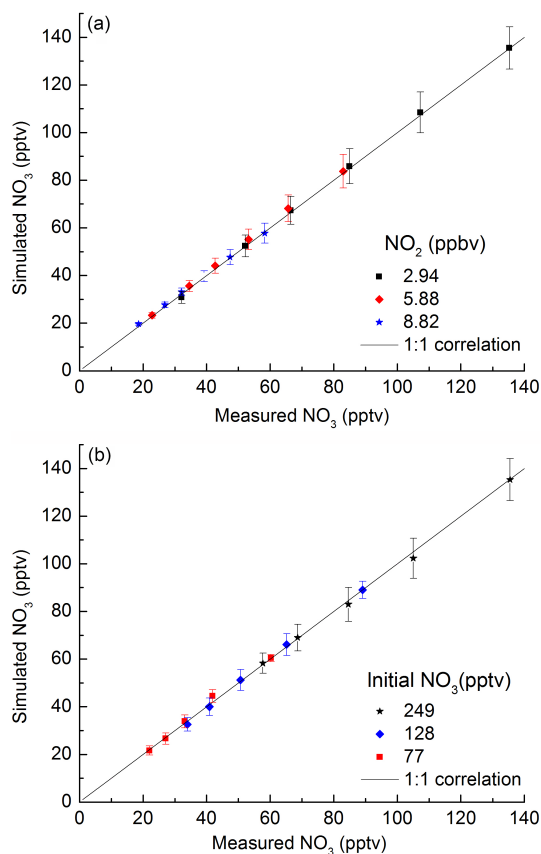
Figure 5. (a) Measured versus simulated NO_3 for different amounts of added NO (67, 134, 201, 268, 402 pptv) and at three different mixing ratios of NO_2. (b) Measured versus simulated NO_3 (initially 77, 128 or 249 pptv) at different amounts (1.5, 3, 4.5, 6 ppbv) of added $[NO_2]$. The solid lines represent 1 : 1 correlation.

below) indicated that the FEP coating did not degrade significantly following sampling of filtered, ambient air. The numerical simulation was initialized with the same set of rate parameters described above, a fixed NO_2 concentration and only k_w and the initial NO_3 concentration were varied. The best fit was obtained when k_w was 4×10^{-3} s^{-1}, in agreement with the simulations at fixed time and variable NO and NO_2. Using Eq. (7) where r is the flow-tube radius, $\bar{c}$ the mean molecular speed and which assumes laminar flow and no diffusive limitation to uptake, this value of k_w can be converted to an approximate uptake coefficient for NO_3 to the FEP-coated tube of $\approx 5 \times 10^{-7}$.

$$\gamma = \frac{2 r k_w}{\bar{c}} \qquad (7)$$

3 Data analysis and derivation of NO₃ reactivity

We first consider the passage of NO_3 through the flow tube in a flow of zero air. If NO_3 is lost in one or more pseudo-
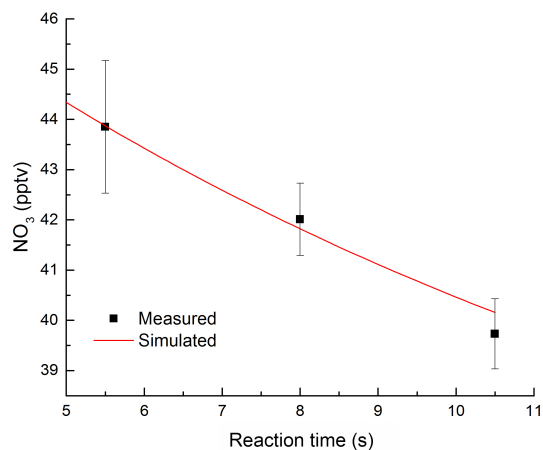

Figure 6. Determination of the NO_3 wall loss constant by variation of the reaction time (injector position). The simulation indicates a wall loss constant of $k_w = 0.004$ s^{-1}.

first-order processes, its decay should be exponential and its concentration, $[NO_3]_t^{ZA}$ after a reaction time t, is given by Eq. (8).

$$[NO_3]_t^{ZA} = [NO_3]_0^{ZA} \exp^{(-k_{ZA} t)}, \qquad (8)$$

where ZA refers to use of zero air. As NO_3 is lost only via reaction with NO_2 and to the wall, $k_{ZA} = k_{wall} + k_{NO_2}$, where k_w is the first-order loss rate constant for wall loss and k_{NO_2} is the first-order loss rate constant for reaction with NO_2 and is equal to $k_3[NO_2]$. When zero air is switched for ambient air containing reactive trace gases, we have

$$[NO_3]_t^{Amb} = [NO_3]_0^{Amb} \exp^{(-k_{Amb} t)}, \qquad (9)$$

where $k_{Amb} = k_w + k_{NO_2} + k_{RTG}$ and k_{RTG} is the first-order loss rate constant for reaction of NO_3 with trace gases present in ambient air other than NO_2.

If $[NO_3]_0^{ZA}$ and $[NO_3]_0^{Amb}$ are equivalent, Eq. 10 is obtained.

$$\frac{[NO_3]_t^{ZA}}{\exp^{(-k_{ZA} t)}} = \frac{[NO_3]_t^{Amb}}{\exp^{(-k_{Amb} t)}} \qquad (10)$$

Rearranging and substituting for k_{ZA} and k_{Amb} leads to

$$k_{RTG} = \frac{\ln\left(\frac{[NO_3]_t^{ZA}}{[NO_3]_t^{Amb}}\right)}{t} = \frac{1}{\tau}, \qquad (11)$$

where τ is the NO_3 lifetime. In principal, it should thus be possible to calculate the reactivity of NO_3 in ambient air by measuring $[NO_3]_t^{ZA}$ and $[NO_3]_t^{Amb}$ and knowing the reaction time t. Later we discuss the applicability of this expression and show that corrections are necessary to take the reformation of NO_3 into account, especially when dealing with air masses with high NO_2 content. This is similar to the laboratory experiments described above and required numerical simulation, which we present below.

The concentration of NO$_3$ in zero air measured when the injector is positioned for maximum reaction time, $[NO_3]_t^{ZA}$, was measured by flushing the inlet with 3000 sccm zero air creating an overflow of $\approx$ 100 sccm. When switching to ambient measurements, the zero-air overflow was redirected via a flow controller (F$_3$ in Fig. 2) that connected the zero-air overflow line to the exhaust and which was set to 3500 sccm. This setup has the advantage of enabling dynamic dilution of ambient air. If the reactivity is so high that the NO$_3$ levels approached the detection limit, F$_3$ does not withdraw the entire 3500 sccm overflow but allows, e.g., 2000 sccm to be added to the inlet, resulting in sampling 900 sccm of ambient air plus 2000 sccm of zero air, a dilution factor of 2900/900 which is slightly increased by the 400 sccm flow from the darkened reactor. A five-point dynamic dilution with zero air is implemented in the software, which changes the set point for F$_3$ and dilutes the ambient air with zero air if $[NO_3]_t^{Amb}$ decreases below 10 pptv for a time period of 30 s. Conversely, the dilution can be decreased again if $[NO_3]_t^{Amb}$ becomes $\geq [NO_3]_t^{ZA} - 10$ ppt. Dilution factors (D_i) were determined using a Gilibrator flow meter (Gilian Gilibrator-2) and were $D_1 = 1.14$ for the measurement of pure ambient air (here the small dilution effect is caused by the 400 sccm zero air used in the production of NO$_3$), $D_2 = 1.74$, $D_3 = 3.71$, $D_4 = 8.98$ and $D_5 = 14.07$ when diluting ambient air. With increasing dilution, errors in the measurement will increase as well (see Sect. 5).

The analytical expression given above to derive the NO$_3$ reactivity is an ideal case in which NO$_3$ is lost by a number of first-order processes and is not formed in the flow tube to a significant extent. However, as we already demonstrated in the laboratory experiments to examine the effects of varying NO, NO$_2$ and NO$_3$ concentrations, the formation of N$_2$O$_5$ in the reaction of NO$_3$ with NO$_2$ (Reaction R3) and its thermal decomposition back to NO$_3$ can impact the NO$_3$ concentration as NO$_2$ is present both in the mixture used to generate N$_2$O$_5$ and NO$_3$ and in ambient air. While the formation of N$_2$O$_5$ from NO$_2$ and NO$_3$ (Reaction R2) is, to a good approximation, independent of temperature between about 280 and 305 K, the rate constant for thermal decomposition of N$_2$O$_5$ (Reaction R3) varies by a factor of 26 over the same temperature range. The simple, analytical approach outlined above thus fails at temperatures where the decomposition of N$_2$O$_5$ is important and when sufficient NO$_2$ is present to account for a significant fraction of the loss of NO$_3$. This is illustrated in Fig. 7a, in which simulations of the NO$_3$ concentration at a reaction time of 10.5 s and at different temperatures and amounts of NO$_2$ (as reactant) are displayed and compared with the simple exponential behavior (black data points) calculated from Eq. (11). The simulations show that the dependence of the NO$_3$ concentration on NO$_2$ is non-exponential, indicating that regeneration of NO$_3$ from the N$_2$O$_5$ formed is significant, especially at higher temperatures. Figure 7b plots the ratio of the true reactivity (i.e., that used as input into the numerical simulation) versus that obtained by ana-
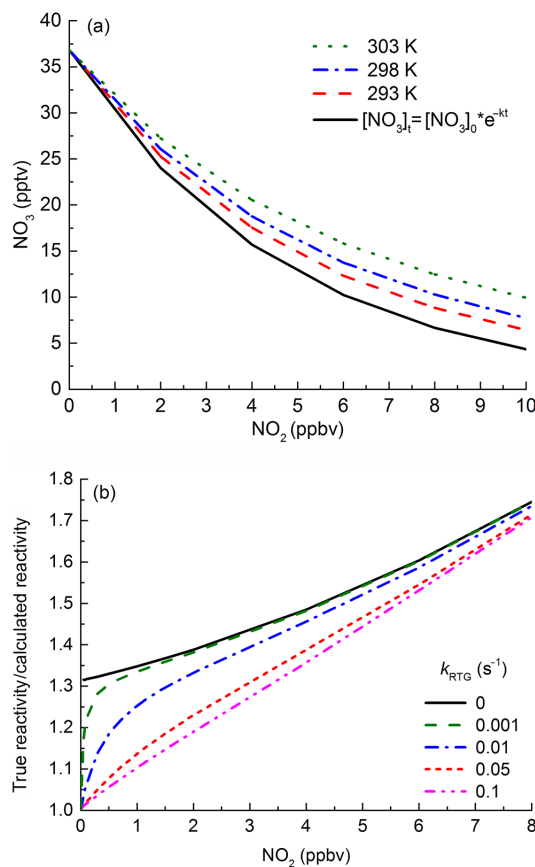

Figure 7. Influence of N$_2$O$_5$ formation and decomposition in the flow tube. **(a)** Simulated (red, blue and green) mixing ratio of NO$_3$ versus added NO$_2$ at a reaction time of 10.5 s at various temperatures and thus thermal decomposition rates of N$_2$O$_5$. The simple exponential decay of NO$_3$ (Eq. 9) is given by the black line. **(b)** Effect of NO$_2$ level on the ratio of true reactivity/reactivity calculated from Eq. (8) for different loss rate constants for NO$_3$ reacting with reactive traces gases.

lyzing the simultaneous change in NO$_3$ concentration using Eq. (11). It is evident that the use of this expression generally results in underestimation of the true reactivity due to the formation and decomposition of N$_2$O$_5$. The bias will be largest when sampling polluted air where the reactivity has a large component due to NO$_2$ and small under conditions of low NO$_2$ and high k_{RTG} typical for remote, forested areas. However, as previously mentioned, the decomposition of N$_2$O$_5$ is strongly temperature dependent so that the bias will increase with rising temperature and decrease with sinking flow-tube temperature.

Apart from the formation and thermal dissociation of N$_2$O$_5$, the reaction of NO$_2$ with O$_3$ may, under some conditions, represent a further potential source of NO$_3$ in the flow tube despite the low rate constant for Reaction (R1). Due to the in situ method of production of N$_2$O$_5$ and NO$_3$ in the dark reactor, NO$_2$ (0.6–3 ppbv) and O$_3$ (40–50 ppbv) are al-
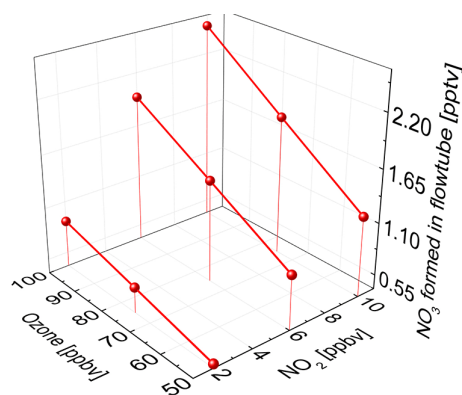
Figure 8. Simulated NO$_3$ production in the flow tube at different O$_3$ and NO$_2$ mixing ratios at a fixed reaction time of 10.5 s.

Figure 9. Raw data showing the change in NO$_3$ (10.5 s reaction time) between zero air (ZA, periods marked with red brackets) and ambient air (Ambient, blue brackets). The figure also shows periods of titration of NO$_3$ with NO ($\approx$ 2 min intervals), a change in the dilution factor from 4 to 3 (at $\approx$ 07:33 UTC) and an in situ reactivity calibration (at $\approx$ 07:07). The "skip" periods are those in which data are not analyzed due to switching from ambient air to zero air and vice versa.

ways present in the flow tube. NO$_3$ generated in the flow tube was therefore simulated for different amounts of O$_3$ and NO$_2$ corresponding to the minimum and maximum mixing ratios used in our experiments. Figure 8 indicates that with 50 ppbv of O$_3$ and 2 ppbv NO$_2$, < 0.5 pptv of NO$_3$ is formed in the 10.5 s available for reaction in the flow tube, which would not strongly impact the results if the analytical expressions above were used to derive the NO$_3$ reactivity. Under highly polluted conditions (e.g., 100 ppbv O$_3$ and 20 ppbv NO$_2$) the effect is, however, measurable (> 2 pptv).

The discussion above indicates that the use of Eq. (11) can, under certain circumstances (e.g., low NO$_x$, high NO$_3$ reactivity to VOCs), give a reasonable representation of the NO$_3$ reactivity. However, in order to be able to derive NO$_3$ reactivities from any air mass we use numerical simulation take NO$_3$ reformation into account and enable extraction of accurate values in any conditions.

Numerical simulations for extraction of ambient reactivity

In this section we outline the experimental procedure and the associated data analysis for extracting the NO$_3$ reactivity from an ambient data set as exemplified by the data shown in Fig. 9. These data cover a 1 h period in which several phases of inlet overfilling with humidified zero air and titration with NO are apparent as are periods of mixing NO$_3$ with ambient air. The data set has already been corrected for baseline drift in the NO$_3$ zero during titration, and hence each titration-zero is scattered around 0 pptv NO$_3$.

The periods marked "ZA" (zero air) were used to extract the NO$_3$ concentration after a residence time of 10.5 s in flow tube in the absence of ambient reactive trace gases. The data show that a plateau in the NO$_3$ signal with zero air is observed after about two–three titration cycles are complete, which is the result of slow flushing through the inlet of reactive gases, which have extended surface residence times on the inlet material and fittings. Once a stable signal is ac-
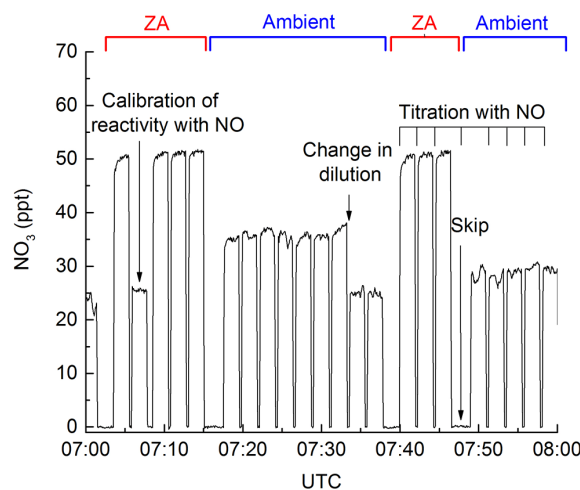
quired, $[NO_3]^{ZA}_{t=10.5}$ can be taken as an average value for each 300s zero-air phase. These values are then used to calculate the initial NO$_3$ concentration $[NO_3]^{ZA}_0$, i.e., before NO$_3$ enters the flow tube. This was done in an iterative procedure using numerical simulation with FACSIMILE embedded in a separate program. Input values are the O$_3$ and NO$_2$ concentration (from the darkened reactor), a first estimate for $[NO_3]^{ZA}_{t=0}$ and the rate coefficients for the NO$_3$ reactions listed in Table 1. At the end of the simulation (a few seconds of computing time) the simulated and measured values of $[NO_3]^{ZA}_{t=10.5}$ are compared and the ratio used to adjust the next input value for $[NO_3]^{ZA}_{t=0}$. The iteration continued until convergence was reached. Convergence was considered satisfactory when the deviation between measured and simulated values of $[NO_3]^{ZA}_{t=10.5}$ was less ≤ 1 %. This usually took only 5 simulations per data point as the initial value for each new time point was chosen to be the final value for the preceding time point. Ideally, $[NO_3]^{ZA}_{t=0}$ should be constant over long periods of time. In fact, deviations of several pptv, especially during field measurements, were observed over periods of hours and so values of $[NO_3]^{ZA}_{t=0}$ were linearly interpolated to each time point in which ambient reactivity was recorded.

Once initial NO$_3$ concentrations had thus been obtained a new set of simulations was started to simulate the measured values of $[NO_3]^{Amb}_{t=10.5}$. In this case, the simulation was initialized with the values of $[NO_3]^{ZA}_{t=0}$ obtained as described above and the total NO$_2$ concentration and O$_3$ concentrations, which contained a constant contribution from the dark reactor and a variable concentration from ambient NO$_2$ and

O$_3$ once corrected by the dilution factor (see above). An initial estimate of the total NO$_3$ reactivity, k_{RTG}, was made and the simulated value of $[NO_3]_{t=10.5}^{Amb}$ compared to that measured. The simulation was iterated, with incremental adjustment of k_{RTG} until agreement between simulation and observation was $\leq 1\%$. For ambient data sets, in which the reactivity can be highly variable, this sometimes took several iterations, though as each simulation took less than a second this is not a particularly time-consuming procedure.

4 Reactivity of an isoprene standard

To validate our experimental and analytical procedure, we performed reactivity measurements on a bottled isoprene standard (0.933 ± 0.09 ppmv, Westfalen), diluted in zero air. Isoprene was chosen as it is an important biogenic reactant for NO$_3$ in the troposphere and also because the rate coefficient, $k_{isoprene}$, for its reaction with NO$_3$ has been studied on many occasions (Atkinson et al., 2006; IUPAC, 2016) and therefore has a low associated uncertainty ($k_{isoprene} = 6.5 \pm 0.15 \times 10^{-13}$ cm^3 molecule^{-1} s^{-1} at 298 K).

Experiments were carried out at various isoprene and NO$_2$ mixing ratios and the results are summarized in Fig. 10, which indicates excellent agreement between the measured reactivity and that calculated from the isoprene mixing ratio and rate coefficient, the slope of an unweighted fit being 1.00 ± 0.03. The error bars on the calculated reactivity represent total uncertainty in the isoprene and NO$_2$ mixing ratio, the reaction time and the rate coefficient. These results confirm that the instrument and data analysis procedure measure accurate values of NO$_3$ reactivity in the presence of NO$_2$ and organic reactants.

5 Detection limit, dynamic range and overall uncertainty

While the overall uncertainty associated with absolute NO$_3$ concentration measurement are influenced by factors such as uncertainty in the cross section as well as in the measurement of the laser emission spectrum, the fractional change in concentration used to derive the NO$_3$ reactivity is not impacted. The detection limit for measuring NO$_3$ reactivity is defined by the minimal detectable change (MDC$_{NO_3}$) in the NO$_3$ mixing ratio. This depends on noise levels and drift in ring-down time, i.e., on the precision of the NO$_3$ signal and also on the stability of the synthetically generated NO$_3$. The instrumental noise on the NO$_3$ signal was reduced by averaging over ≈ 3 s per data point (≈ 1800 ring-down events) to give a noise-limited detection limit (1σ) of ~ 0.2 pptv. Precision is limited by the stability of the CRDS setup where changes in the mirror reflectivity induced by thermal or mechanical stress can lead to a drift in the ring-down time. The precision can be estimated from the standard deviation of the
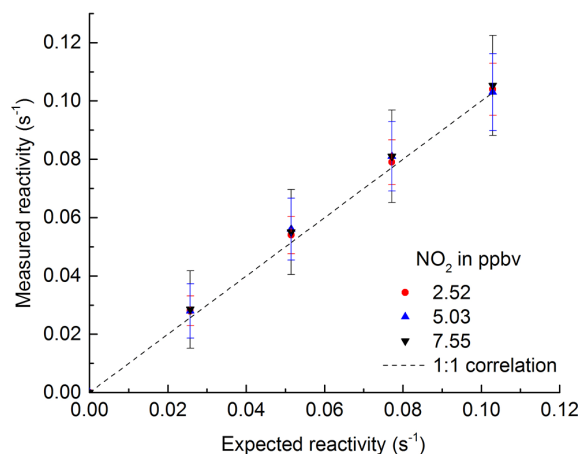

Figure 10. Verification of the experimental procedure by addition of isoprene at different NO$_2$ mixing ratios. The known reactivity was calculated from the isoprene mixing ratio (1.5–6 ppbv) and the rate coefficient for reaction of isoprene with NO$_3$. Experiments were performed in dry zero air. The error bars in the simulation are due to uncertainties in [isoprene] and [NO$_2$] (both 5 %) and the reaction time (10 %).

signal from one zeroing period to the next over the measurement period. Under typical laboratory conditions this was normally ≈ 0.7 pptv.

Since $[NO_3]_0^{ZA}$ is interpolated onto the measured $[NO_3]_t^{Amb}$ time series to calculate the reactivity, the stability of the NO$_3$ source is of great importance. Changes in the amount of synthetically generated NO$_3$ are caused by fluctuations in the temperature or pressure of the dark reactor, the flow of NO$_2$ and changes in the intensity of light from the O$_3$ generator. In general, the poorer the stability of the NO$_3$ source chemistry, the more frequently the NO$_3$ mixing ratio in zero air has to be measured. In laboratory conditions, changes of ± 1 pptv within 1 h were typical, making $[NO_3]_t^{ZA}$ measurements every 1200 s more than sufficient. In field conditions, where the instrument housing may be subject to larger temperature fluctuations, more frequent determination of $[NO_3]_t^{ZA}$ may be necessary. The NO$_3$ source stability was obtained from the standard deviation of the averaged $[NO_3]_t^{ZA}$ concentrations and propagating this with the standard deviation of two consecutive $[NO_3]_t^{ZA}$ measurements, for which typical values in laboratory conditions were ≈ 1 ppt. To define an overall, minimal detectable change in NO$_3$ (MDC$_{NO_3}$), the noise- and drift-limited precision was combined with the NO$_3$ source stability to result in MDC$_{NO_3} = 2.5$ pptv.

An MDC$_{NO_3}$ of 2.5 pptv results in a lower limit for the measurement of NO$_3$ reactivity of 0.005 s^{-1} (obtained from Eq. 11 with $[NO_3]_t^{ZA} = 50$ pptv and $[NO_3]_t^{Amb} = [NO_3]_t^{ZA} - $ MDC$_{NO_3} = 47.5$ pptv, at the lowest dilution factor of 1.14). An upper limit for the measurable reactivity is 45 s^{-1}, largely defined by the uncertainty of the dilution factor. Dilution fac-

tors were obtained by measurements of the actual flows going into the flow tube using a Gilibrator flow meter (Gilian Gilibrator-2, stated accuracy ±1 %). The total uncertainty in the dilution factor is defined by the accuracy of the measurement of the dilution flows as well as by the accuracy of the flow controllers used for flow regulation (±2 %) and was calculated to be 2.5 %. The error in the calculated reactivity is lowest for the lowest dilution but if the $[NO_3]_t^{Amb}$ gets close to the detection limit this will also have a strong influence on the calculated reactivities making a higher dilution factor favorable. Dilution factors were chosen to keep the instrument operating in a region (10 pptv < NO$_3$ < 40 pptv) where both effects are minimized.

A minimum detectable change in NO$_3$ of 2.5 pptv leads to an uncertainty of ≈ 15 %, when NO$_3$ varies between ≈ 10 and 30 pptv (starting from 50 pptv in zero air). The uncertainty increases dramatically when NO$_3$ levels are close to 50 pptv (i.e., very low reactivity) or less than 5 pptv (very high reactivity without dilution). This is illustrated in Fig. S1 of the Supplement. As mentioned in Sect. 2.3 the uncertainty in the reaction time (10 %) also contributes to the overall uncertainty.

To assess the uncertainty associated with derivation of the NO$_3$ reactivity from numerical simulation, uncertainties associated with the input parameters have to be considered. As previously demonstrated (Groß et al., 2014) this is best assessed in a Monte Carlo approach in which the key parameters are varied within a range reflecting their uncertainty limits. The parameters that most sensitively influence the derived value of NO$_3$ reactivity are the NO$_2$ mixing ratio and the rate coefficients for N$_2$O$_5$ formation ($k_3 = 1.2 \pm 0.1 \times 10^{-12}$ cm^3 molecule^{-1} s^{-1}) and decomposition ($k_4 = 4.4 \pm 0.4 \times 10^{-2}$ cm^3 molecule^{-1} s^{-1}). The rate coefficients listed are for 1 bar and room temperature as appropriate for the experimental conditions, the uncertainties quoted (≈ 10 %) are based on assessment of kinetic data (Burkholder et al., 2016). The Monte Carlo simulations were initiated with a NO$_3$ mixing ratio (in zero air) of 50 pptv, decreasing to 20 pptv upon reaction with air. In total, six sets of ≈ 1200 simulations were carried with variation of the initial NO$_2$ mixing ratio between 1 and 5 ppbv and the associated error in NO$_2$ mixing ratio was taken as 8 %. For any given simulation, the output value of the NO$_3$ reactivity (k_{RTG}) was stored. The 2σ uncertainty was derived from the Gaussian fits to histograms of k_{RTG} (insets at NO$_2$ = 1.0, 3.0 and 5.0 ppbv) and is plotted (as a percent of k_{RTG}) versus k_{RTG}/NO$_2$. The latter may be considered a measure of whether NO$_3$ reacts predominantly with NO$_2$ to form N$_2$O$_5$ (k_3) or with reactive trace gases. Figure 11 shows that the uncertainty associated with the simulations is very sensitive to ambient NO$_2$ levels, varying between > 100 % (at 5 ppbv NO$_2$ and a reactivity of 0.017 s^{-1}) and 3.1 % (at 1 ppbv NO$_2$ and a reactivity of 0.092 s^{-1}) of the extracted k_{RTG}. Clearly, the extraction of k_{RTG} is most accurate in conditions of low NO$_x$ and when
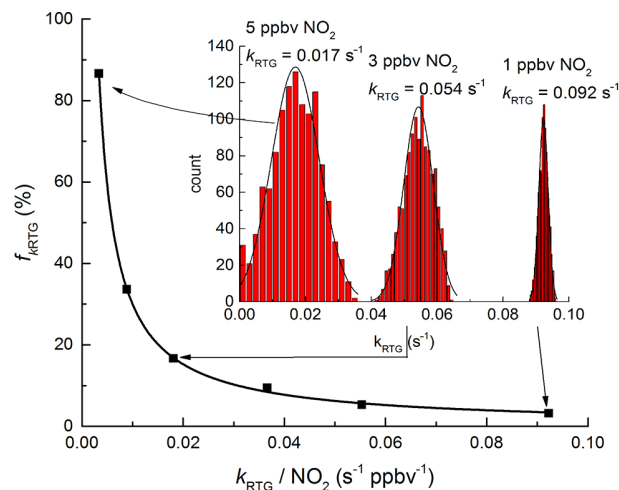

Figure 11. Uncertainty factor (f k_{RTG}) as a function of the ratio k_{RTG}/ [NO$_2$] as derived from Monte Carlo simulations. The relationship (black line) is described by f (k_{RTG}) = 0.33 × (k_{RTG}/[NO$_2$])$^{-0.977}$. The results of three individual sets of 1200 simulations are shown as histograms.

NO$_3$ lifetimes are short (e.g., forested regions far from anthropogenic activity).

Another potential bias in the measurement is the temperature dependence of the rate constant of the reactions of trace gases with NO$_3$. Measurements were normally conducted at 20 °C in the flow tube whilst outside temperature can differ from this. However, (unlike OH) the NO$_3$ reactions which dominate its reactivity involve addition to double bonds (e.g., of terpenes) and are only weakly temperature dependent. Therefore, to a good approximation, this error can generally be neglected. To illustrate this, we consider the reaction between NO$_3$ and the usually most abundant monoterpene, α-pinene. The rate constant at the flow-tube temperature (20 °C) is 6.4×10^{-12}, increasing to 7.0×10^{-12} cm^3 molecule^{-1} s^{-1} at 5 °C and decreasing to 5.9×10^{-12} cm^3 molecule^{-1} s^{-1} at 35 °C, which are changes of < 10 %. Note also that for many monoterpenes, the temperature dependence of the rate constant is not known but expected to be weak (IUPAC, 2016).

Under circumstances where the reactivity is known to be driven by reaction with reactive trace gases for which NO$_3$ has large temperature dependence this error has to be taken into consideration.

We now examine the potential bias caused by use of NO$_3$ concentrations as large as 50 pptv, which may change the reactivity of the air either by removing a significant fraction of gas-phase reactants or via formation of peroxy radicals (RO$_2$), which may also react with NO$_3$. In a first scenario, we assume that the reactivity is caused by a single species, namely the generally dominant terpene, α-pinene and consider both low (k_{RTG} = 0.005 s^{-1}) and high reactivity regimes (k_{RTG} = 0.1 s^{-1}). A value of k_{RTG} = 0.005 s^{-1}

would result if 34 pptv of α-pinene were available for reaction. In a first approximation, assuming first-order kinetics, we calculate that 2.5 pptv of the initially available 50 pptv of NO$_3$ is lost in the 10.5 s reaction time, and consequently a change in α-pinene of 2.5 pptv would also occur. This is only 7 % of the initial concentration, indicating an upper limit to a negative bias of 7 %. This is an upper limit, as the assumption of first-order kinetics is not entirely appropriate. As NO$_3$ reacts with α-pinene in air to form a nitrooxyperoxy radical (RO$_2$) we also consider a positive bias due to reaction of NO$_3$ with this RO$_2$. To do this we assume a rate constant of 1.2×10^{-12} cm^3 molecule^{-1} s^{-1} for the reaction as observed for NO$_3 +$ CH$_3$O$_2$ (Atkinson et al., 2006) and assume that this rate constant is approximately independent of the nature of the organic fragment (R) as is the case for reactions of RO$_2$ with NO. The 2.5 pptv RO$_2$ thus generated results in an incremental NO$_3$ reactivity of 7×10^{-5} s^{-1}, a positive bias of 1.5 %. Again, this is an upper limit, as the calculation assumes that this concentration of RO$_2$ is constant and available for the whole 10.5 s of reaction time. For higher reactivity (0.1 s^{-1}) a similar calculation shows that the 670 pptv required would reduce the NO$_3$ concentration to 17.5 pptv, itself being diminished to ~ 640 pptv, a change of just 5 %. The 32.5 pptv RO$_2$ generated would result in a loss rate constant for NO$_3$ of $\sim 9 \times 10^{-4}$ s^{-1}, a positive bias of ~ 1 %. In conclusion, for reactive systems in which a large concentration of reactive trace gases with moderate reactivity towards NO$_3$ are encountered, we expect no significant bias. The only scenario in which a large bias can ensue is when a low reactivity is caused by a very low concentration of an extremely reactive traces gas. Taking the example of 1 pptv of a highly reactive terpenoid ($k = 2 \times 10^{-10}$ cm^3 molecule^{-1} s^{-1}) it is easy to show that it would be reduced to just a few percent of its initial concentration when mixed with 50 pptv of NO$_3$ for 10.5 s. In this case a large negative bias would result. In the real atmosphere, this situation is however unlikely to occur as such reactive species are usually substantially reduced in concentration compared to the generally dominant biogenics such as α-pinene.

The overall uncertainty thus derives from a combination of measurement errors (cavity instability, drift in NO$_3$ source, etc.) and the need to correct for NO$_3$ reactions with NO$_2$. Under ideal conditions (e.g., as described above for laboratory operation) the former can be reduced to ≈ 16 %. For a scenario in which biogenic VOCs dominate NO$_3$ reactivity in a low NO$_x$ (< 1 ppbv) environment an additional uncertainty of ≈ 6–10 % from the numerical simulations results in a total uncertainty of ≈ 17–20 %. In a high-NO$_x$ environment, the total uncertainty will be dominated by that associated with the simulations. For example, at 5 ppbv NO$_2$ and a reactivity of 0.03 s^{-1} the total error would be close to 45–50 %.
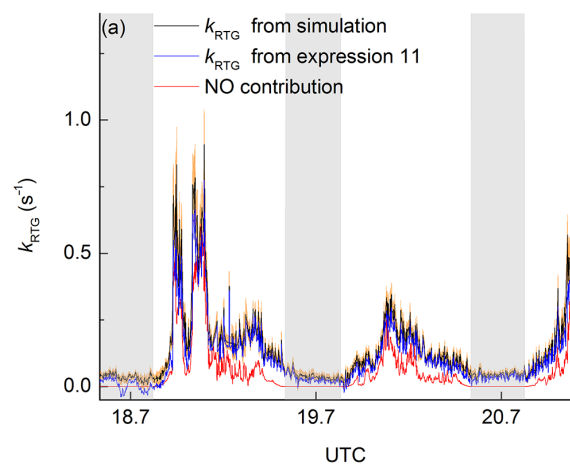

Figure 12. Measured values of k_{RTG} over a 3-day period. The overall uncertainty is represented by the amber, shaded area. The black lines are k_{RTG} obtained by full simulations; the blue lines are calculated using Eq. (11) (without correction for N$_2$O$_5$ formation and decomposition). The contribution of NO to the NO$_3$ reactivity is displayed as the red line. Grey shaded regions correspond to night-time; ticks are at midnight.

6 Deployment in the NOTOMO campaign, 2015

The NO$_3$ reactivity setup described above was deployed for the first time in the field during the NOTOMO campaign in the Taunus mountains (southwestern Germany) in 2016. The site, previously described in detail (Crowley et al., 2010; Sobanski et al., 2016b), is situated on top of the "Kleiner Feldberg" mountain (850 m above sea level) in a forested area with urban influence. The site is impacted by biogenic emissions from forested regions (mainly in the northwest) and by anthropogenic emissions from the local urban centers of Frankfurt, Mainz and Wiesbaden in the southeast to southwest.

Reactivity measurements during NOTOMO

The NO$_3$ reactivity instrument was located in a research container and sampled from a common high-flow inlet together with other instruments. The high-flow inlet was driven by an industrial fan drawing 10 m^3 min^{-1} through a 15 cm diameter stainless steel pipe with its opening about 8 m above the ground. This flow was sub-sampled with a 4 m length of 1/4 in. PFA tubing that extracted the required 3300 sccm air from the center of the stainless steel pipe and directed it through a 2 μm PFA filter to the NO$_3$-reactivity instrument. Due to thermostat breakdown during NOTOMO, the NO$_3$-reactivity measurements were performed with the flow tube at container temperature, which was variable (14–31 °C).

Previous campaigns at the Taunus Observatory have revealed occasionally high nighttime mixing ratios of NO$_3$ and N$_2$O$_5$ (Sobanski et al., 2016b). As sampling NO$_3$ and N$_2$O$_5$ from ambient air would bias the NO$_3$-reactivity measure-

ments to low values, a 2 L glass flask heated to ≈ 40–$50\,^{\circ}$C was placed at night in the ambient air stream to decompose N$_2$O$_5$ to NO$_3$ and NO$_2$. Based on its thermal dissociation rate coefficient ($0.75\,\mathrm{s}^{-1}$ at $50\,^{\circ}$C), N$_2$O$_5$ completely decomposes within the $\approx 40\,\mathrm{s}$ residence time in this glass vessel, and the NO$_3$ formed is expected to be lost on the uncoated glass walls, thus preventing reformation of N$_2$O$_5$. Measurements with ≈ 200 pptv of N$_2$O$_5$ added directly to the heated vessel and measured by the ambient and heated channels of the two-cavity CRDS (see Sect. 2.2) confirmed that neither NO$_3$ nor N$_2$O$_5$ survived. As the N$_2$O$_5$ mixing ratio was measured during NOTOMO it is in principal possible to correct the data for the additional NO$_2$ thus generated. However, on most nights N$_2$O$_5$ levels were too low for this to have a significant effect. Further experiments with isoprene and α-pinene indicated that there was no significant change in NO$_3$ reactivity when the glass vessel was used or not, indicating no significant losses of these VOCs in the glass flask. We cannot exclude that other, less volatile organic trace gases including, e.g., acids or peroxides may be lost in the glass vessel, but these are not expected to contribute significantly to NO$_3$ losses as their rate coefficients for reaction with NO$_3$ are generally too low. A further potential bias related to the use of the glass trap is the thermal decomposition of PAN and related peroxy nitrates, which can acquire concentrations of up to a few ppb at this site (Sobanski et al., 2016c; Thieser et al., 2016). If PAN decomposes in the glass vessel NO$_2$ will form, thus contributing to the measured reactivity. Simulations indicate that during the 40 s residence time in the heated flask (at $50\,^{\circ}$C) only a small fraction ($\approx 2.6\,\%$) of the PAN decomposes to form NO$_2$. For future experiments in environments of high NO$_x$ with N$_2$O$_5$ and NO$_3$ present, the glass trap will be operated at a lower temperature (e.g., $35\,^{\circ}$C, $\tau_{\mathrm{PAN}} = \sim 500\,\mathrm{s}$, $\tau_{\mathrm{N_2O_5}} = \sim 6\,\mathrm{s}$) to make sure all of the N$_2$O$_5$/NO$_3$ is removed but PAN is preserved. We note that when measuring NO$_3$ reactivity in regions with large biogenic emissions, the use of the glass vessel to remove NO$_3$ and N$_2$O$_5$ is generally not necessary as high levels of biogenic VOCs and the low levels of NO$_x$ often found in forested/rural environments remote from anthropogenic influence will result in very low levels of NO$_3$ or N$_2$O$_5$.

During NOTOMO, ambient levels of NO$_2$, NO$_3$, N$_2$O$_5$ and organic nitrates were measured with the CRDS instruments previously described by Sobanski et al. (2016a; Thieser et al., 2016). The uncertainty in the measurements was 8 % for NO$_2$ and 20 % for NO$_3$, whereas the uncertainty for PAN was highly variable for each data point (Sobanski et al., 2016c). The O$_3$ mixing ratios were measured using a dual beam ozone monitor (2B Technology model 205) with an uncertainty of 2 %. [NO] was not directly measured but its daytime concentration was calculated assuming photo-stationary state via Eq. (12):

$$[\mathrm{NO}]_{\mathrm{calc}} = \frac{J(\mathrm{NO_2})[\mathrm{NO_2}]}{k_{(\mathrm{NO+O_3})}[\mathrm{O_3}]} \qquad (12)$$

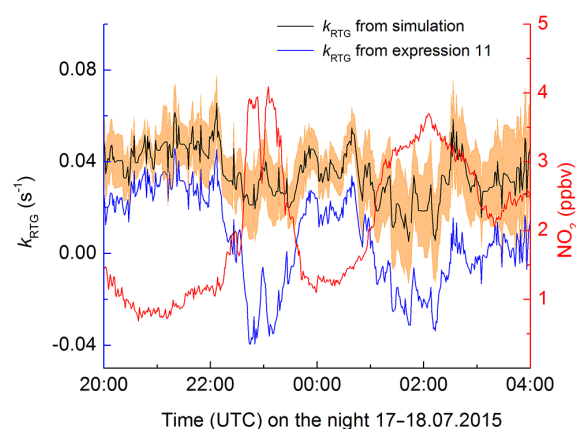**Figure 13.** Zoom in on a nighttime period with low reactivity emphasizing the effect of NO$_2$-induced formation and decomposition of N$_2$O$_5$.
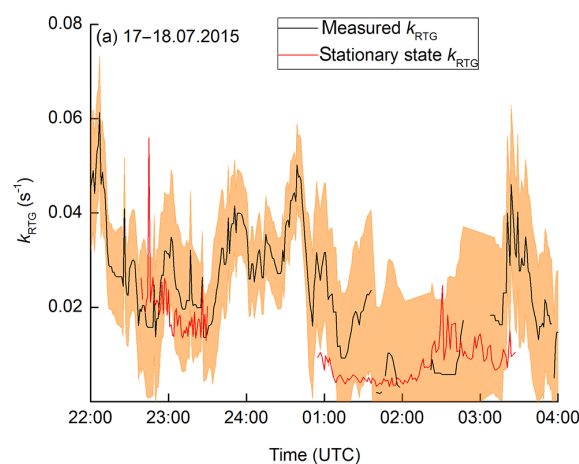

Figure 14. Comparison of stationary-state and measured NO$_3$ loss rates on two nights (17–18 July and 18–19 July 2015). Uncertainty in k_{RTG} (see text) is displayed as the amber shaded area.

where $J(\mathrm{NO_2})$ is the photolysis frequency of NO$_2$ and $k_{(\mathrm{NO+O_3})}$ is the rate constant for reaction of NO with O$_3$. This expression ignores the oxidation of NO to NO$_2$ via, e.g., reactions of peroxy radicals and thus overestimates NO. $J(\mathrm{NO_2})$ was measured using a spectral radiometer located close to the inlet (MetCon).

In this paper we focus on a 3-day period, during which NO$_3$ reactivity was measured (Fig. 12). The NO$_3$ reactivity, k_{RTG}, varied from 0.005 to $0.1\,\mathrm{s}^{-1}$ during nighttime but reached values as high as $1.4\,\mathrm{s}^{-1}$ during daytime. The total uncertainty of the measurement is depicted by the amber, shaded area. The red line indicates that daytime losses are dominated by reaction with NO (up to $1.3\,\mathrm{s}^{-1}$). Nighttime values of k_{RTG} were between 0.005 and $0.1\,\mathrm{s}^{-1}$. Assuming that NO levels are close to zero as measured previously at this site during nighttime (Crowley et al., 2010), k_{RTG} is then expected to be dominated by VOCs.

In Fig. 13, we compare values of k_{RTG} obtained by rigorous data correction (black curve) to those calculated directly from Eq. (11) (blue curve). The simple analytical expression (blue line) results in an underestimation of the reactivity, especially during night, when the overall reactivity is low, and in periods of high [NO$_2$]. Owing to lack of temperature stabilization of the darkened reactor (at this time not yet incorporated) and breakdown of the flow-tube thermostat during the campaign, temperature fluctuations in the container resulted in MDC$_{\mathrm{NO_3}}$ = 5.6 pptv and hence an average, lowest measurable reactivity of $\approx 0.01\,\mathrm{s}^{-1}$ during the campaign. As described in Sect. 5 the minimum detectable change in NO$_3$ was combined with the uncertainty associated with the dilution factor, reaction time, [NO$_2$], [PAN] and rate constants used to calculate the overall uncertainty for the reactivity at every data point. The overall uncertainty for the measurement period illustrated in Fig. 13 was $\approx 25\,\%$.

In Fig. 14, we compare the measured nighttime NO$_3$ reactivity with that obtained from the stationary-state analysis using Eq. (1). For the two nights in the period analyzed, NO$_3$ mixing ratios were between 5 and 37 pptv and the calculated stationary-state loss rate coefficients varied between 0.03 and $0.003\,\mathrm{s}^{-1}$ compared to the measured reactivity which was between 0.05 and $0.006\,\mathrm{s}^{-1}$ with a short time period in which k_{RTG} fell below the detection limit of the instrument. Within the total uncertainty, the measured and stationary-state reactivities are in reasonable agreement for most of the night from the 17 to the 18 July. From the night 18 to the 19 July the stationary-state reactivity is much lower (up to a factor of 8) than that measured. This difference and also the higher variability can be attributed to rapid variations in concentrations of VOCs at the inlet (due, e.g., to emissions from nearby trees) that are not considered in the stationary-state approach; i.e., very local emissions of reactive gases will result in breakdown of the stationary-state assumption, leading to the underestimation of the reactivity of the local mixture of VOCs and NO$_x$. As the direct measurement of the NO$_3$ reactivity with this device sums over all VOCs present in the air mass sampled, it should give the same result as summing each VOC concentration multiplied by the individual rate coefficients for reaction with NO$_3$, i.e NO$_3$ reactivity $= \Sigma[\mathrm{VOC}]_i k_i$. As demonstrated previously for this mountain site (Sobanski et al., 2016b), summed losses based on measurement of VOCs can significantly exceed the reactivity based on a stationary-state analysis especially under some meteorological situations in which a low-lying residual layer (with high NO$_3$ concentrations) influences the measurement.

7   Conclusion and outlook

We present the first instrument for measurement of NO$_3$ reactivity in ambient air. The flow-tube-based instrument utilizes the depletion of synthetically generated NO$_3$ when mixed with ambient air and has a dynamic range of 0.005 to $45\,\mathrm{s}^{-1}$.

Following intensive laboratory characterization to determine the effective reaction time, the wall loss constant of NO$_3$ and the effect of NO$_3$ formation and reformation in the flow tube, it was successfully tested against an isoprene standard. The overall uncertainty depends on the relative rate of reaction of NO$_3$ with NO$_2$ or with other traces gases (e.g., VOCs or NO) that do not generate N$_2$O$_5$ and which, under ideal conditions, is close to 15 %. The instrument is thus best suited for measurement of NO$_3$ reactivity in regions with high biogenic activity and relatively low direct anthropogenic emissions of NO$_x$, i.e., regions where the measurement of NO$_3$ concentrations is difficult owing to low production rates and a high loss term.

First deployment of the instrument was during the NOTOMO observational experiment in summer 2015 at a forested, mountain site with urban influence. The measured NO$_3$ reactivity ranged from 0.006 to 0.1 tos^{-1} at nighttime and reached values as high as $1.4\,\mathrm{s}^{-1}$ during daytime. As expected, daytime reactivity was dominated by reaction with NO while nighttime reactivity involved other (presumably organic) trace gases. A comparison with stationary-state calculations of the NO$_3$ reactivity revealed occasional poor agreement, presumably related to very local emissions causing a breakdown of the stationary-state assumption.

Improvements to the dynamic range of the instrument require further stabilization of the NO$_3$ source and cavity optics to reduce the minimal detectable change in NO$_3$ (presently MDC$_{\mathrm{NO_3}}$ = 2.5 pptv). This could also be achieved by the use of larger volume flow tubes. Reduction in the initial NO$_3$ concentration used would also reduce any potential bias caused by depletion of reactants or secondary chemistry. Future deployment with simultaneous measurements of NO$_3$, NO$_2$, O$_3$ and VOCs will be conducted to compare direct measurements of NO$_3$ reactivity with those obtained from the stationary-state approach and also those calculated from summing losses due to individual VOCs.

The Supplement related to this article is available online at doi:10.5194/amt-10-1241-2017-supplement.

References

Atkinson, R.: Atmospheric chemistry of VOCs and NO$_x$, Atmos. Environ., 34, 2063–2101, 2000.

Atkinson, R. and Arey, J.: Gas-phase tropospheric chemistry of biogenic volatile organic compounds: a review, Atmos. Environ., 37, S197–S219, 2003a.

Atkinson, R. and Arey, J.: Atmospheric degradation of volatile organic compounds, Chem. Rev., 103, 4605–4638, doi:10.1021/cr0206420, 2003b.

Atkinson, R., Baulch, D. L., Cox, R. A., Crowley, J. N., Hampson, R. F., Hynes, R. G., Jenkin, M. E., Rossi, M. J., and Troe, J.: Evaluated kinetic and photochemical data for atmospheric chemistry: Volume I – gas phase reactions of O$_x$, HO$_x$, NO$_x$ and SO$_x$ species, Atmos. Chem. Phys., 4, 1461–1738, doi:10.5194/acp-4-1461-2004, 2004.

Atkinson, R., Baulch, D. L., Cox, R. A., Crowley, J. N., Hampson, R. F., Hynes, R. G., Jenkin, M. E., Rossi, M. J., Troe, J., and IUPAC Subcommittee: Evaluated kinetic and photochemical data for atmospheric chemistry: Volume II – gas phase reactions of organic species, Atmos. Chem. Phys., 6, 3625–4055, doi:10.5194/acp-6-3625-2006, 2006.

Berden, G., Peeters, R., and Meijer, G.: Cavity ring-down spectroscopy: Experimental schemes and applications, Int. Rev. Phys. Chem., 19, 565–607, 2000.

Brown, S. S. and Stutz, J.: radical observations and chemistry, Chem. Soc. Rev., 41, 6405–6447, 2012.

Brown, S. S., Stark, H., and Ravishankara, A. R.: Cavity ring-down spectroscopy for atmospheric trace gas detection: application to the nitrate radical (NO$_3$), Appl. Phys. B-Lasers O., 75, 173–182, 2002.

Brown, S. S., Stark, H., and Ravishankara, A. R.: Applicability of the steady state approximation to the interpretation of atmospheric observations of NO$_3$ and N$_2$O$_5$, J. Geophys. Res.-Atmos., 108, 4539, doi:10.1029/2003JD003407, 2003.

Brown, S. S., Dube, W. P., Osthoff, H. D., Stutz, J., Ryerson, T. B., Wollny, A. G., Brock, C. A., Warneke, C., De Gouw, J. A., Atlas, E., Neuman, J. A., Holloway, J. S., Lerner, B. M., Williams, E. J., Kuster, W. C., Goldan, P. D., Angevine, W. M., Trainer, M., Fehsenfeld, F. C., and Ravishankara, A. R.: Vertical profiles in NO$_3$ and N$_2$O$_5$ measured from an aircraft: Results from the NOAA P-3 and surface platforms during the New England Air Quality Study 2004, J. Geophys. Res.-Atmos., 112, D22304, doi:10.1029/2007jd008893, 2007a.

Brown, S. S., Dubé, W. P., Osthoff, H. D., Wolfe, D. E., Angevine, W. M., and Ravishankara, A. R.: High resolution vertical distributions of NO$_3$ and N$_2$O$_5$ through the nocturnal boundary layer, Atmos. Chem. Phys., 7, 139–149, doi:10.5194/acp-7-139-2007, 2007b.

Brown, S. S., Dube, W. P., Fuchs, H., Ryerson, T. B., Wollny, A. G., Brock, C. A., Bahreini, R., Middlebrook, A. M., Neuman, J. A., Atlas, E., Roberts, J. M., Osthoff, H. D., Trainer, M., Fehsenfeld, F. C., and Ravishankara, A. R.: Reactive uptake coefficients for N$_2$O$_5$ determined from aircraft measurements during the Second Texas Air Quality Study: Comparison to current model parameterizations, J. Geophys. Res.-Atmos., 114, D00F10, doi:10.1029/2008JD011679, 2009.

Burkholder, J. B., Sander, S. P., Abbatt, J., Barker, J. R., Huie, R. E., Kolb, C. E., Kurylo, M. J., Orkin, V. L., Wilmouth, D. M., and Wine, P. H.: Chemical Kinetics and Photochemical Data for Use in Atmospheric Studies, Evaluation No. 18, JPL Publication 15-10, Jet Propulsion Laboratory, Pasadena, USA, available at: http://jpldataeval.jpl.nasa.gov, 2016.

Crowley, J. N., Schuster, G., Pouvesle, N., Parchatka, U., Fischer, H., Bonn, B., Bingemer, H., and Lelieveld, J.: Nocturnal nitrogen oxides at a rural mountain-site in south-western Germany, Atmos. Chem. Phys., 10, 2795–2812, doi:10.5194/acp-10-2795-2010, 2010.

Crowley, J. N., Thieser, J., Tang, M. J., Schuster, G., Bozem, H., Beygi, Z. H., Fischer, H., Diesch, J.-M., Drewnick, F., Borrmann, S., Song, W., Yassaa, N., Williams, J., Pöhler, D., Platt, U., and Lelieveld, J.: Variable lifetimes and loss mechanisms for NO$_3$ and N$_2$O$_5$ during the DOMINO campaign: contrasts between marine, urban and continental air, Atmos. Chem. Phys., 11, 10853–10870, doi:10.5194/acp-11-10853-2011, 2011.

Crutzen, P.: A discussion of the chemistry of some minor constituents in the stratosphere and troposphere, Pure Appl. Geophys., 106–108, 1385–1399, 1973.

Curtis, A. R. and Sweetenham, W. P.: Facsimile, AERE, Report R-12805, Harwell Laboratory, Oxfordshire, UK, 1987.

Dentener, F. J. and Crutzen, P. J.: Reaction of N$_2$O$_5$ on tropospheric aerosols – Impact on the global distributions of NO$_x$, O$_3$, and OH, J. Geophys. Res.-Atmos., 98, 7149–7163, 1993.

Donahue, N. M., Clarke, J. S., Demerjian, K. L., and Anderson, J. G.: Free-radical kinetics at high pressure: A mathematical analysis of the flow reactor, J. Phys. Chem., 100, 5821–5838, 1996.

Fry, J. L., Draper, D. C., Barsanti, K. C., Smith, J. N., Ortega, J., Winkle, P. M., Lawler, M. J., Brown, S. S., Edwards, P. M., Cohen, R. C., and Lee, L.: Secondary Organic Aerosol Formation and Organic Nitrate Yield from NO$_3$ Oxidation of Biogenic Hydrocarbons, Environ. Sci. Technol., 48, 11944–11953, doi:10.1021/es502204x, 2014.

Fuchs, H., Dube, W. P., Cicioira, S. J., and Brown, S. S.: Determination of inlet transmission and conversion efficiencies for in situ measurements of the nocturnal nitrogen oxides, NO$_3$, N$_2$O$_5$ and NO$_2$, via pulsed cavity ring-down spectroscopy, Anal. Chem., 80, 6010–6017, 2008.

Geyer, A. and Platt, U.: Temperature dependence of the NO$_3$ loss frequency: A new indicator for the contribution of NO$_3$ to the oxidation of monoterpenes and NO$_x$ removal in the atmosphere, J. Geophys. Res.-Atmos., 107, 4431, doi:10.1029/2001JD001215, 2002.

Groß, C. B. M., Dillon, T. J., Schuster, G., Lelieveld, J., and Crowley, J. N.: Direct kinetic study of OH and O$_3$ formation in the reaction of CH$_3$C(O)O$_2$ with HO$_2$, J. Phys. Chem. A, 118, 974–985, doi:10.1021/jp412380z, 2014.

Guenther, A. B., Jiang, X., Heald, C. L., Sakulyanontvittaya, T., Duhl, T., Emmons, L. K., and Wang, X.: The Model of Emissions of Gases and Aerosols from Nature version 2.1 (MEGAN2.1): an extended and updated framework for modeling biogenic emissions, Geosci. Model Dev., 5, 1471–1492, doi:10.5194/gmd-5-1471-2012, 2012.

Heintz, F., Platt, U., Flentje, H., and Dubois, R.: Long-term observation of nitrate radicals at the tor station, Kap Arkona (Rugen), J. Geophys. Res.-Atmos., 101, 22891–22910, 1996.

Howard, C. J.: Kinetic measurements using flow tubes, J. Phys. Chem., 83, 3–9, 1979.

Huang, Y., Shen, H. Z., Chen, Y. L., Zhong, Q. R., Chen, H., Wang, R., Shen, G. F., Liu, J. F., Li, B. G., and Tao, S.: Global organic carbon emissions from primary sources from 1960 to 2009, Atmos. Environ., 122, 505–512, doi:10.1016/j.atmosenv.2015.10.017, 2015.

Huang, Y., Coggon, M. M., Zhao, R., Lignell, H., Bauer, M. U., Flagan, R. C., and Seinfeld, J. H.: The Caltech Photooxidation Flow Tube reactor: design, fluid dynamics and characterization, Atmos. Meas. Tech., 10, 839–867, doi:10.5194/amt-10-839-2017, 2017.

IUPAC: Task Group on Atmospheric Chemical Kinetic Data Evaluation, Ammann, M., Cox, R. A., Crowley, J. N., Herrmann, H., Jenkin, M. E., McNeill, V. F., Mellouki, A., Rossi, M. J., Troe, J. and Wallington, T. J., available at: http://iupac.pole-ether.fr/index.html, last access: November 2016.

Kovacs, T. A. and Brune, W. H.: Total OH loss rate measurement, J. Atmos. Chem., 39, 105–122, doi:10.1023/a:1010614113786, 2001.

Lelieveld, J., Butler, T. M., Crowley, J. N., Dillon, T. J., Fischer, H., Ganzeveld, L., Harder, H., Lawrence, M. G., Martinez, M., Taraborrelli, D., and Williams, J.: Atmospheric oxidation capacity sustained by a tropical forest, Nature, 452, 737–740, 2008.

Lelieveld, J., Gromov, S., Pozzer, A., and Taraborrelli, D.: Global tropospheric hydroxyl distribution, budget and reactivity, Atmos. Chem. Phys., 16, 12477–12493, doi:10.5194/acp-16-12477-2016, 2016.

Mielke, L. H., Furgeson, A., and Osthoff, H. D.: Observation of ClNO$_2$ in a mid-continental urban environment, Environ. Sci. Technol., 45, 8889–8896, doi:10.1021/es201955u, 2011.

Mogensen, D., Gierens, R., Crowley, J. N., Keronen, P., Smolander, S., Sogachev, A., Nölscher, A. C., Zhou, L., Kulmala, M., Tang, M. J., Williams, J., and Boy, M.: Simulations of atmospheric OH, O$_3$ and NO$_3$ reactivities within and above the boreal forest, Atmos. Chem. Phys., 15, 3909–3932, doi:10.5194/acp-15-3909-2015, 2015.

Ng, N. L., Brown, S. S., Archibald, A. T., Atlas, E., Cohen, R. C., Crowley, J. N., Day, D. A., Donahue, N. M., Fry, J. L., Fuchs, H., Griffin, R. J., Guzman, M. I., Herrmann, H., Hodzic, A., Iinuma, Y., Jimenez, J. L., Kiendler-Scharr, A., Lee, B. H., Luecken, D. J., Mao, J., McLaren, R., Mutzel, A., Osthoff, H. D., Ouyang, B., Picquet-Varrault, B., Platt, U., Pye, H. O. T., Rudich, Y., Schwantes, R. H., Shiraiwa, M., Stutz, J., Thornton, J. A., Tilgner, A., Williams, B. J., and Zaveri, R. A.: Nitrate radicals and biogenic volatile organic compounds: oxidation, mechanisms, and organic aerosol, Atmos. Chem. Phys., 17, 2103–2162, doi:10.5194/acp-17-2103-2017, 2017.

Orphal, J., Fellows, C. E., and Flaud, P. M.: The visible absorption spectrum of NO$_3$ measured by high-resolution Fourier

transform spectroscopy, J. Geophys. Res.-Atmos., 108, 4077, doi:10.1029/2002JD002489, 2003.

Osthoff, H. D., Pilling, M. J., Ravishankara, A. R., and Brown, S. S.: Temperature dependence of the NO$_3$ absorption cross-section above 298 K and determination of the equilibrium constant for NO$_3$ + NO$_2$ <-> N$_2$O$_5$ at atmospherically relevant conditions, Phys. Chem. Chem. Phys., 9, 5785–5793, 2007.

Osthoff, H. D., Roberts, J. M., Ravishankara, A. R., Williams, E. J., Lerner, B. M., Sommariva, R., Bates, T. S., Coffman, D., Quinn, P. K., Dibb, J. E., Stark, H., Burkholder, J. B., Talukdar, R. K., Meagher, J., Fehsenfeld, F. C., and Brown, S. S.: High levels of nitryl chloride in the polluted subtropical marine boundary layer, Nat. Geosci., 1, 324–328, 2008.

Phillips, G. J., Tang, M. J., Thieser, J., Brickwedde, B., Schuster, G., Bohn, B., Lelieveld, J., and Crowley, J. N.: Significant concentrations of nitryl chloride observed in rural continental Europe associated with the influence of sea salt chloride and anthropogenic emissions, Geophys. Res. Lett., 39, L10811, doi:10.1029/2012GL051912, 2012.

Riedel, T. P., Bertram, T. H., Crisp, T. A., Williams, E. J., Lerner, B. M., Vlasenko, A., Li, S. M., Gilman, J., de Gouw, J., Bon, D. M., Wagner, N. L., Brown, S. S., and Thornton, J. A.: Nitryl Chloride and Molecular Chlorine in the Coastal Marine Boundary Layer, Environ. Sci. Technol., 46, 10463–10470, doi:10.1021/es204632r, 2012.

Rinne, J., Markkanen, T., Ruuskanen, T. M., Petäjä, T., Keronen, P., Tang, M. J., Crowley, J. N., Rannik, Ü., and Vesala, T.: Effect of chemical degradation on fluxes of reactive compounds – a study with a stochastic Lagrangian transport model, Atmos. Chem. Phys., 12, 4843–4854, doi:10.5194/acp-12-4843-2012, 2012.

Schuster, G., Labazan, I., and Crowley, J. N.: A cavity ring down/cavity enhanced absorption device for measurement of ambient NO$_3$ and N$_2$O$_5$, Atmos. Meas. Tech., 2, 1–13, doi:10.5194/amt-2-1-2009, 2009.

Seeley, J. V., Jayne, J. T., and Molina, M. J.: High-Pressure Fast-Flow Technique for Gas-Phase Kinetics Studies, Int. J. Chem. Kinet., 25, 571–594, 1993.

Sinha, V., Williams, J., Crowley, J. N., and Lelieveld, J.: The Comparative Reactivity Method – a new tool to measure total OH Reactivity in ambient air, Atmos. Chem. Phys., 8, 2213–2227, doi:10.5194/acp-8-2213-2008, 2008.

Sobanski, N., Schuladen, J., Schuster, G., Lelieveld, J., and Crowley, J. N.: A five-channel cavity ring-down spectrometer for the detection of NO$_2$, NO$_3$, N$_2$O$_5$, total peroxy nitrates and total alkyl nitrates, Atmos. Meas. Tech., 9, 5103–5118, doi:10.5194/amt-9-5103-2016, 2016a.

Sobanski, N., Tang, M. J., Thieser, J., Schuster, G., Pöhler, D., Fischer, H., Song, W., Sauvage, C., Williams, J., Fachinger, J., Berkes, F., Hoor, P., Platt, U., Lelieveld, J., and Crowley, J. N.: Chemical and meteorological influences on the lifetime of NO$_3$ at a semi-rural mountain site during PARADE, Atmos. Chem. Phys., 16, 4867–4883, doi:10.5194/acp-16-4867-2016, 2016b.

Sobanski, N., Thieser, J., Schuladen, J., Sauvage, C., Song, W., Williams, J., lieleveld, J., and Crowley, J. N.: Day- and Night-time Formation of Organic Nitrates at a Forested Mountain-site in South West Germany, Atmos. Chem. Phys. Discuss., accepted, 2016c.

Thieser, J., Schuster, G., Schuladen, J., Phillips, G. J., Reiffs, A., Parchatka, U., Pöhler, D., Lelieveld, J., and Crowley, J. N.: A

two-channel thermal dissociation cavity ring-down spectrometer for the detection of ambient NO$_2$, RO$_2$NO$_2$ and RONO$_2$, Atmos. Meas. Tech., 9, 553–576, doi:10.5194/amt-9-553-2016, 2016.

Thornton, J. A., Kercher, J. P., Riedel, T. P., Wagner, N. L., Cozic, J., Holloway, J. S., Dube, W. P., Wolfe, G. M., Quinn, P. K., Middlebrook, A. M., Alexander, B., and Brown, S. S.: A large atomic chlorine source inferred from mid-continental reactive nitrogen chemistry, Nature, 464, 271–274, doi:10.1038/nature08905, 2010.

Wagner, N. L., Dubé, W. P., Washenfelder, R. A., Young, C. J., Pollack, I. B., Ryerson, T. B., and Brown, S. S.: Diode laser-based cavity ring-down instrument for NO$_3$, N$_2$O$_5$, NO, NO$_2$ and O$_3$ from aircraft, Atmos. Meas. Tech., 4, 1227–1240, doi:10.5194/amt-4-1227-2011, 2011.

Wayne, R. P., Barnes, I., Biggs, P., Burrows, J. P., Canosa-Mas, C. E., Hjorth, J., Le Bras, G., Moortgat, G. K., Perner, D., Poulet, G., Restelli, G., and Sidebottom, H.: The nitrate radical: Physics, chemistry, and the atmosphere, Atmos. Environ. A, 25A, 1–206, 1991.